Arch. Metall. Mater. **68** (2023), 3, 895-905

DOI: https://doi.org/10.24425/amm.2023.145453

M. KAPTANOGLU[1*], M. EROGLU[1]

INVESTIGATION OF HARDFACING DEPOSITS OBTAINED BY USING SUBMERGED ARC WELDING FLUXES CONTAINING HIGH-CARBON FERROCHROMIUM AND FERROBORON

Hardfacing deposition processes were carried out using unalloyed S1-EL12 welding wire and submerged arc welding fluxes produced by agglomerated method containing 4-16 wt.% ferrochromium and 2 wt.% ferroboron to achieve wear-resistant of hardfacing deposits on common steel substrates via submerged arc welding. Typical parameters such as slag detachment behaviour, measurements of weld seam widths and heights, microstructural examinations, and hardness and wear tests of hardfacing deposits were characterized. End of the characterization processes, with the increase of chromium, carbon, and boron transition from welding fluxes to hardfacing deposits, the welding seam widths, and heights were determined to increase from 14.12 mm to 15.65 mm and 6.14 mm to 6.50 mm, respectively. Besides; carbide and boro-carbide ratios in the microstructures increased, the hardness values increased from 43 HRC to 61 HRC and the wear losses decreased from 5.79 to 4.43. (10^{-7} mm^3 (N m)$^{-1}$).

Keywords: Submerged arc welding; Hardfacing deposit; Carbide; Boro-carbide; Welding flux

1. Introduction

Worn and corroded materials encounter mechanical losses during their lifetime. Renewal of such kinds of materials with a new material poses a problem in terms of both production processes and costs [1]. Accordingly, damaged materials are coated to extend service life using a variety of methods, such as thermal spray (HVOF) [2], laser [3], electric arc welding [4], and the like. In the thermal spray method, special powder particles prepared for coating are aimed to fill worn surfaces under high pressure, speed, and temperature. While this method is advantageous in terms of being a fast process and applying to different types of materials, it has a disadvantage in terms of its high cost and low filling capacity. In laser applications, metallic materials and compounds in powder form are adhered to the surface of the material to be coated by using various methods such as gas atomization, and a coating layer is formed on the surface via laser energy. While this method has advantages such as speed and compatibility with fabrication, high cost is the most important disadvantage of the method. In electric arc welding methods, it is aimed to obtain hardfacing deposits by the use of alloyed electrodes and/or metallic powders. In some cases, while electric arc welding methods are advantageous in terms of having a relatively high filling capacity and cost-effectiveness, the need for operator experience and the limited number of alloyed or cored wires for each technique are the disadvantages of the method. But, in electric arc methods such as submerged arc welding, the main advantage is the minimum heat loss during the process, which is, at the same time it is the main disadvantage, due to the high dilution and the wide heat affected zone underneath. Therefore, all arc welding techniques can have advantages and disadvantages. The studies using the electric arc welding method in the literature have been conducted by the techniques such as Gas Tungsten Arc Welding (GTAW) [5], Gas Metal Arc Welding (GMAW) [6], Flux Cored Arc Welding (FCAW) [7], plasma transferred arc (PTAW) [8] and Submerged Arc Welding (SAW) [9]. In the studies conducted using the electric arc welding methods, hardfacing deposits are generally carried out by using alloyed welding wires [7]. In these hardfacing deposits, the welding wire (electrode) plays an important role in determining the character, microstructure, hardness, and wear resistance of the hardfacing deposits. In the literature, the researchers aiming to apply hardfacing deposit via electric arc welding method have preferred to perform hardfacing deposit by using the welding techniques other than submerged arc welding technique. In the limited number of hardfacing deposition studies conducted by submerged arc welding technique [4,9-12], the researchers have performed the hardfacing deposits by using alloyed/unalloyed

[1] UNIVERSITY OF FIRAT, FACULTY OF ENGINEERING, DEPARTMENT OF METALLURGICAL AND MATERIALS ENGINEERING, ELAZIG, 23000, TURKEY

* Corresponding author:mkaptanoglu@firat.edu.tr

wire and unalloyed welding flux combinations by laying metallic powders on the surface to be coated. In these types of applications, the most important problems are laying the metallic powders on the surface to be coated at the optimum level and mixing the powders homogeneously, especially in circular cross-section materials. In addition, laying metallic powders on the surface to be coated causes an extra-time loss and experimental setup requirement [4,9,10,12]. For these reasons, this study aims to obtain hardfacing deposits by using alloyed submerged arc welding fluxes (powders) produced via the agglomeration method [13]. As it is well-known, the main task of submerged arc welding fluxes is to protect the welding bath from the harmful effects of air and to determine the geometry of the welding metal by forming slags during the welding process. In addition to these tasks, the aim of this study is also to contribute to the hardfacing deposit production by using ferroalloys in submerged arc welding fluxes. Due to the use of unalloyed welding wire in the hardfacing deposition processes, it is mainly intended to pass alloying elements from the welding fluxes to the hardfacing deposits. In this context, the feasibility of hardfacing deposits obtained using welding fluxes containing increasing amounts of ferrochromium and ferroboron was investigated on iron-based materials, which are thicker than 3 mm and have flat and circular geometry.

2. Experimental procedure

2.1. Agglomerated welding flux production

Submerged arc welding fluxes are produced by using melting or agglomeration methods [13]. In the present study, submerged arc welding fluxes for the aim of hardfacing deposits were produced by the agglomerated submerged arc welding flux production method due to the ease of production and the availability of using ferroalloys. The flow chart of welding fluxes production is given in Fig. 1. The agglomerated submerged arc welding fluxes were produced by using silicon dioxide (SiO_2), magnesium oxide (MgO), aluminum oxide (Al_2O_3), calcium fluoride (CaF_2), calcium oxide (CaO), titanium dioxide (TiO_2), manganese oxide (MnO), potassium oxide (K_2O), sodium oxide (Na_2O) and the ferroalloys ferromanganese (FeMn), ferromolybdenum (FeMo), ferrochromium (FeCr) and ferroboron (FeB) (TABLE 1). To reduce the production costs, the slag waste of the ferrochromium plant of Elazig, Turkey contains 31.2 wt.% SiO_2, 33.7 wt.% MgO, 29.9 wt.% Al_2O_3, 2.6 wt.% Cr_2O_3, 1.45 wt.% CaO, 0.9 wt.% FeO was added into the welding flux mixtures. The formulated welding fluxes compositions and basicity index given in TABLE 1 have been preferred since the slag forming powder components are more compatible with ferroalloys and the slag formers can fulfill the welding powder duties optimally. Besides, to give the hardfacing character to the welding fluxes, 4-16 wt.% FeCr and 2 wt.% FeB were added into the flux mixtures and welding fluxes were produced. Ferrochromium and ferroboron alloys have been preferred since economical compounds occur from iron, chromium, carbon, and boron with high wear resistance and high hardness up to 1400-1600 HV can be obtained by using ferroboron and ferrochromium in welding powders [13]. The used ferroboron, ferrochromium, ferromanganese, and ferromolybdenum chemical compositions are given in TABLE 2.

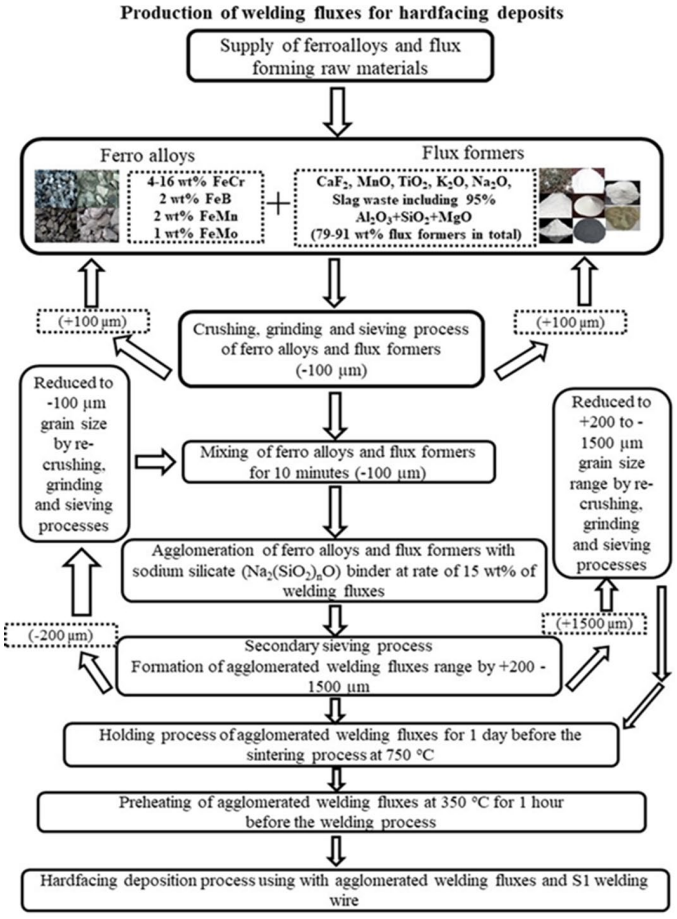

Fig. 1. FLow chart of welding fluxes production for hardfacing deposits

TABLE 1

Chemical compositions of welding fluxes prepared for hardfacing deposits

Flux numbers	Basicity index*	Chemical composition (wt.%)									
		CaF_2	CaO	TiO_2	MnO	$Na_2O + K_2O$	Slag	FeCr	FeB	FeMn	FeMo
# 1	1.28	10	5	6	5	1.5	63.5	4	2	2	1
# 2	1.30	10	5	6	5	1.5	59.5	8	2	2	1
# 3	1.35	10	5	6	5	1.5	55.5	12	2	2	1
# 4	1.39	10	5	6	5	1.5	51.5	16	2	2	1

* The basicity index was calculated with the help of the following Boniszewski formula.
BI = $(CaO + CaF_2 + MgO + K_2O + Na_2O + Li_2O + BaO + SrO + 0.5MnO + 0.5FeO) / (SiO_2 + 0.5Al_2O_3 + 0.5TiO_2 + 0.5ZrO_2)$

TABLE 2

Chemical composition of ferroalloys used in flux production

Material	Chemical composition (wt.%)					
FeCr	Cr	C	Si	S	P	Fe
	65(±2)	8(±0.5)	1.1(±0.1)	0.004(±0.001)	0.010(±0.005)	Bal.
Material	Chemical composition (wt.%)					
FeB	B	C	Si	Al	Fe	
	18(±0.5)	0.25(±0.01)	0.25(±0.01)	0.07(±0.01)	Bal.	
Material	Chemical composition (wt.%)					
FeMn	Mn	C	Si	S	P	Fe
	74(±2)	1.5(±0.1)	1.2(±0.1)	0.022(±0.001)	0.12(±0.01)	Bal.
Material	Chemical composition (wt.%)					
FeMo	Mo	C	Si	S	P	Fe
	63(±2)	0.1(±0.01)	1(±0.1)	0.04 (max)	0.05 (max)	Bal.

In the production of agglomerated welding fluxes, firstly, the flux components were reduced to –100 micron grain size via the crushing, grinding, and sieving processes, respectively [14]. Then, the welding fluxes reduced to –100 micron grain size were mixed to be as homogeneous as possible for ten minutes in the compositions given in TABLE 1. The fluxes mixed in a special mixer were agglomerated by using a sodium silicate ($Na_2(SiO_2)_nO$) binder at a rate of 15 wt.% of the flux mixture. After this process, these fluxes were sintered for one hour at 750°C [13]. Agglomerated fluxes, which reached the targeted flux strength by sintering, were subjected to re-crushing, grinding, and sieving processes in the range between +200 µm-1500 µm. The fluxes with +200 µm-1500 µm grain sizes have a hygroscopic character and this behavior affects the welding quality negatively. Therefore, these agglomerated welding fluxes were preheated at 350°C for 1 hour before the hardfacing deposition process [13].

2.2. Hardfacing deposition processes

Hardfacing deposition processes were performed by using a Magmaweld MZC-1000 model submerged arc welding machine with a ZD5-1000B model power unit. In all hardfacing deposition processes, welding wire (electrode) which was obtained from Magmaweld company in Turkey, had a 3.2-mm wire diameter, and was coded with SW 701 in AWS/ASME SFA-5.17 EL12 standard (EN ISO 14171-A S1) were used. The chemical composition of this wire [15] is given in TABLE 3. This welding wire was used together with submerged arc welding fluxes during the hardfacing deposition processes.

TABLE 3

Chemical composition of AISI 1020 steel and S1 welding wire used in hardfacing deposition processes

Material	Chemical composition (wt.%)					
AISI 1020 steel	C	Si	Mn	P	S	Fe
	0.15	0.28	0.64	0.03	0.03	Bal.
Material	Chemical composition (wt.%)					
S1 welding wire	C	Si	Mn	Fe		
	0.07	0.05	0.50	Bal.		

Hardfacing deposits were applied on AISI (American Iron & Steel Institute) 1020 steel surfaces in sizes of 10×30×600 mm, the chemical composition of which is given in TABLE 3. The steel material surfaces were cleaned from all kinds of dirt and rust before the hardfacing deposition processes. In all the hardfacing deposition processes, the welding parameters specified in TABLE 4 were used. Before the chemical and microstructural analyses, superficial crack and porosity examinations were performed by using the Liquid Penetrant Test method [16]. In addition, the seam width and height, and the melting depth of the hardfacing deposits were measured by using a metallurgical microscope interfaced with an image analysis system. On the other hand, the slag properties of the welding fluxes and the surface properties of the hardfacing deposits were checked by visual analyses with the naked eye.

TABLE 4

SAW machine parameters used in hardfacing deposition processes

Current (A)	Voltage (V)	Welding speed ($cm \cdot min^{-1}$)	Wire diameter (mm)	Electrode polarity (±)	Stick-out (mm)
500	28	50	3.2	+	32

2.3. Microstructure, XRD, and chemical composition analyses

Dimensionally and visually examined hardfacing deposit samples # 1-4 were cut in sizes of 14×10×10 mm to determine the chemical composition and microstructure analyses without allowing any thermal effect in the Tronic brand EcoCut 85V model laboratory type wet cutting and turning machine (Fig. 2). The samples # 1-4 cut was subjected to sanding, polishing, and etching processes via classical metallographic methods. In the etching process, nital (98 vol.% ethyl alcohol + 2 vol.% nitric acid) solutions were used and the range time for etching of each sample lasted 5 minutes on average. In the microscopic examinations of the etched samples, Nikon branded Eclipse-MA200i model optic microscope and Jeol branded JSM-7001F Inca X-Act model scanning electron microscope (SEM-15 kV) were used. To

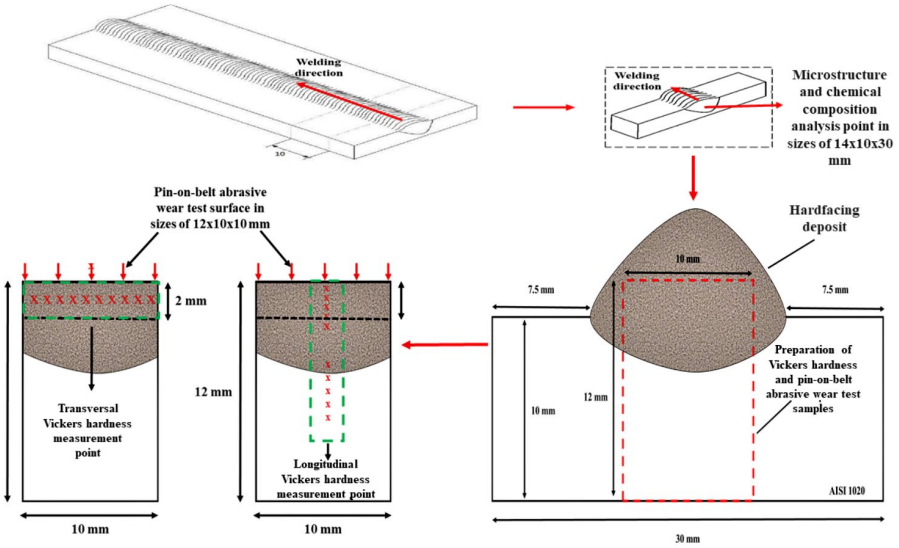

Fig. 2. The preparation of test samples and their application points

determine the phases in the microstructures, X-ray analyses were performed by using the Rigaku brand RadB-Dmax2 model device with CuKα radiation at room temperature. Similarly, inductively coupled plasma atomic emission spectrometer (ICP-AES), and Jeol brand JXA-8230 model EPMA-EDS devices were used for the analyses of the chemical composition. ICP-AES samples were prepared in powder form and used to determine the percentage amounts of elements other than carbon, while EPMA-EDS samples were prepared in bulk form and used to determine the percentage amount of carbon.

2.4. Hardness and abrasive wear tests

To measure the Rockwell and Vickers hardness of the hardfacing deposits with an average weld seam length of 20 cm, 2 samples with the cross-sectional dimensions of 12×10×10 mm were prepared. The prepared samples were taken from the midpoints of the coatings. Rockwell hardness measurements were performed under 150 kgf loads according to the C scale of the Rockwell hardness measurement method (HRC) by using an EMCO M4U-025 model hardness measuring device. The Vickers hardness measurements were made under 200 gr loads ($HV_{0.2}$) via the Leica MHT-10 hardness measuring device. Rockwell hardness measurements were performed by calculating the mean of the hardness values taken from 10 different zones of the hardfacing deposits. Vickers hardness measurements were made according to the measurements taken from 10 different transverse and longitudinal areas (Fig. 2).

For abrasive wear tests, samples # 1-4 were cut in the size of 12×10×10 mm (Fig. 2) and they were subjected to the ASTM-G132-96 pin-on-belt abrasive wear test method [17]. A schematic representation of the pin-on-abrasive belt wear test method was given in Fig. 3. The hardfacing deposits for wear tests were dimensionally equalized by using cutting and turning machines such as hardness test samples. In the wear tests, band sandpapers with a length of 920 mm and a width of 100 mm were used and the wear tests were performed by using the Buehler Surfmet I device. The wear tests were performed under 80 mesh sandpaper, 20-newton load, 50 m sliding distance, and 300 rpm speed with room temperature. Wear losses were calculated by measuring the weights before and after the experimental tests, comparisons were made by taking the wear rate as a basis, and new sandpapers were used in each test. Since the surfacing layers are considered an average iron alloy, the hardfacing deposit densities were determined as 7.85 ($gr \cdot cm^{-3}$).

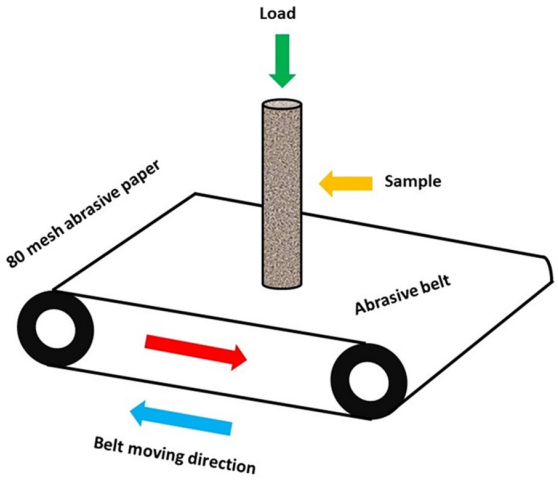

Fig. 3. Schematic representation of the pin-on-belt abrasive wear test method

3. Results and discussion

3.1. Visual and dimensional analysis results

Fig. 4a-d shows images of the hardfacing deposits obtained by welding fluxes containing ferrochromium and ferroboron with increasing rates. When the agglomerated fluxes given in were

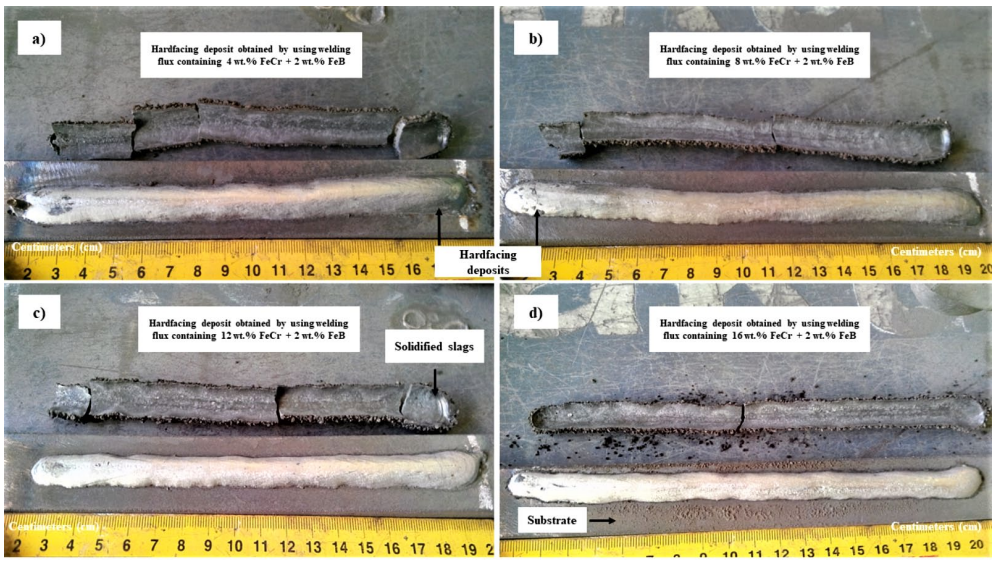

Fig. 4. Images of hardfacing deposits and slags. a) sample # 1, b) sample # 2, c) sample # 3, d) sample # 4

examined, it was observed that the grain sizes of welding fluxes were in the range of +300-500 µm according to Rosin-Rammler distribution [18] and they had similar sizes. This situation was associated with the use of a 15 wt.% binder in all the welding flux mixtures and having similar compositions with each other except for ferroalloys. Also, it was observed that the fluxes had a characteristically similar appearance since all the fluxes were produced via the agglomeration method and were subjected to the same grain sizing process.

When the hardfacing deposit samples # 1-4 were examined via the Liquid Penetrant Test and the naked eye in terms of superficial cracks and porosities, it was determined that there were no cracks or porosities in all 4 hardfacing deposits. This situation was correlated to the good preservation of the hardfacing layer by the welding fluxes, the suitability of the grain size of the fluxes, the suitability of the deoxidizing ferroalloy amounts in the fluxes, and the suitability of the flux formulas.

When the welding seam widths and heights of the hardfacing deposit samples # 1-4 were compared, it was determined that the welding seam widths and heights partially increased with the increase of FeCr and FeB compounds in welding fluxes (TABLE 5). The widths of the welding seam increased from 14.12 mm to 15.65 mm and the heights of the welding seam increased from 6.14 mm to 6.50 mm were determined as an average. Similarly, the increase in the amount of alloying elements in the fluxes caused the melting depth to decrease from 4.42 mm to 4.17 mm. These results were also compatible with the commercial product technical specifications obtained by the brands such as Lincoln Electric, ESAB, and Magmaweld (Oerlikon) which are leading in the welding industry [19-21]. On the other hand, the homogeneity of the welding seams partially decreased depending on the increasing alloying element percentages in hardfacing deposits. This phenomenon was associated with the characteristics of the ferroalloys in hardfacing deposits.

When samples # 1-4 given in Fig. 4a-d were assessed in terms of the self-removal characteristic of the slag, it was determined that the self-removal characteristic of the slags was decreased in general due to the increasing percentage of ferroalloys in welding fluxes. In particular, at the highest ferrochromium-ferroboron rates (welding flux example # 4), it was observed that the slag had difficulty detaching from the hardfacing deposit and had a tendency to stick to the hardfacing deposit. This phenomenon was associated with the ferroalloy behaviour, interfacial tension, and phase transformation during the cooling [22]. On the other hand, in samples # 1-3, it was observed that there were no obvious problems with the removal of slags from the weld metals (hardfacing deposits) spontaneously. But, the removal times of the slags from the weld metals increased with the increasing percentage of ferroalloys in welding fluxes and this situation did not cause such a problem as in sample # 4.

TABLE 5

Welding seam widths and heights, and melting depths of hardfacing deposits

Hardfacing deposit samples	Mean values of welding seam width (mm)	Mean values of welding seam height (mm)	Mean values of melting depth (mm)
# 1	14.12±4	6.14±3	4.42±3
# 2	14.26±5	6.18±4	4.36±2
# 3	15.11±4	6.38±3	4.25±4
# 4	15.65±6	6.50±5	4.17±3

3.2. Chemical composition, microstructure, and XRD analysis results

TABLE 6 shows the chemical composition analysis results obtained from the hardfacing deposit samples # 1-4. According to TABLE 6, 1.54-6.84 wt.% chromium, 0.38-0.44 wt.% boron, and 0.87-1.08 wt.% carbon transition from welding fluxes to the hardfacing deposits were determined. While the highest

TABLE 6

Chemical composition analysis results of hardfacing deposits obtained by ICP-AES and EPMA-EDS

Hardfacing deposit numbers	Chemical composition (wt.%)						
	Cr	C	Mn	Mo	Si	B	Fe
# 1	1.54	0.87	1.03	0.16	0.20	0.38	Bal.
# 2	3.25	0.98	0.88	0.17	0.21	0.41	Bal.
# 3	5.45	1.03	1.02	0.16	0.21	0.43	Bal.
# 4	6.84	1.08	1.03	0.19	0.19	0.44	Bal.

chromium, boron, and carbon transition was observed in hardfacing deposit obtained with welding flux containing 16 wt.% ferrochromium and 2 wt.% ferroboron, the lowest chromium, boron, and carbon transition was observed in hardfacing deposit obtained with welding flux containing 4 wt.% ferrochromium and 2 wt.% ferroboron. Furthermore, it was determined that all the hardfacing deposits contained an average of 0.20 wt.% silicon and 1 wt.% manganese and molybdenum. The amount of alloying elements transferred to the hardfacing deposits was associated with the reducing potential of carbon in deoxidant character at high temperature and the use of deoxidants ferromanganese and ferrosilicon in flux bodies [23-25].

The microstructure images of the hardfacing deposits samples #1 and # 4 were shown in Fig. 5-8, respectively. Phases formed in the microstructures were austenite (γ iron), Fe_3C (cementite), $(Fe,Cr)_{23}C_6$, and $(Fe,Cr)_7BC_4$. These phases forming in the microstructures were supported by XRD (Fig. 9), chemical composition analyses (TABLE 6), and the literature [4,6,9,26-30], and it was determined that these and similar phases could be formed depending on the quantity of iron, chromium, boron, and carbon. Since a great majority of the studies in the literature were carried out by the arc welding techniques other than the submerged arc welding technique, the results of the present study were correlated with the results of studies carried out with different arc welding techniques and also a limited number of studies carried out with submerged arc welding technique.

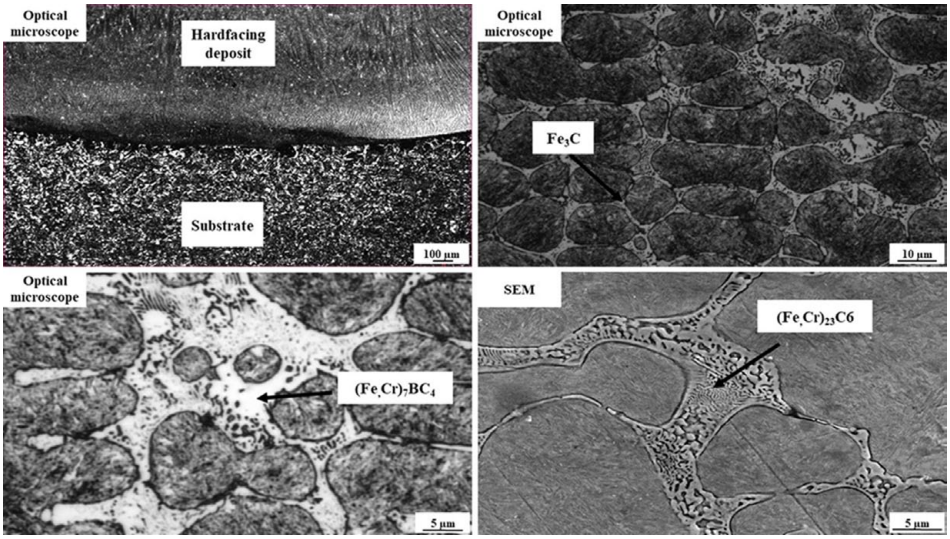

Fig. 5. Optical microscope and SEM microstructure images of hardfacing deposit sample # 1

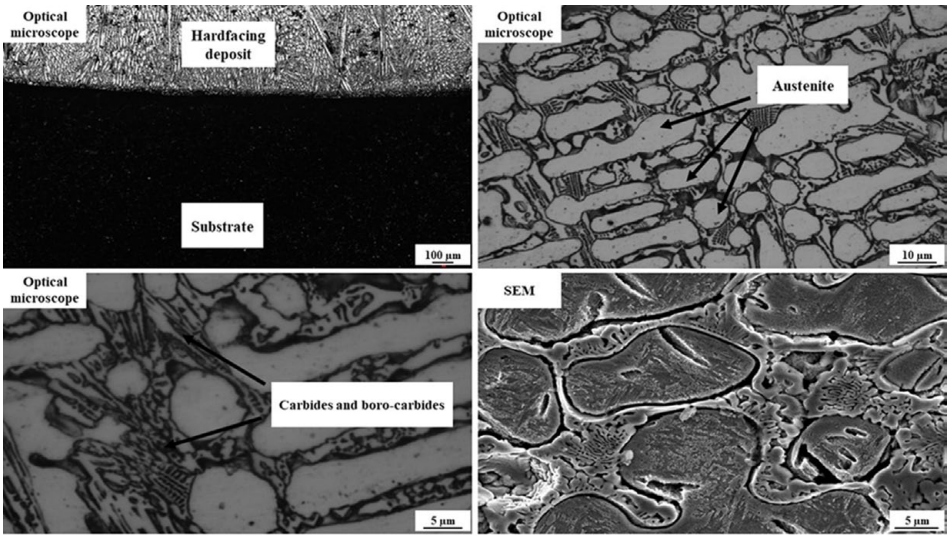

Fig. 6. Optical microscope and SEM microstructure images of hardfacing deposit sample # 2

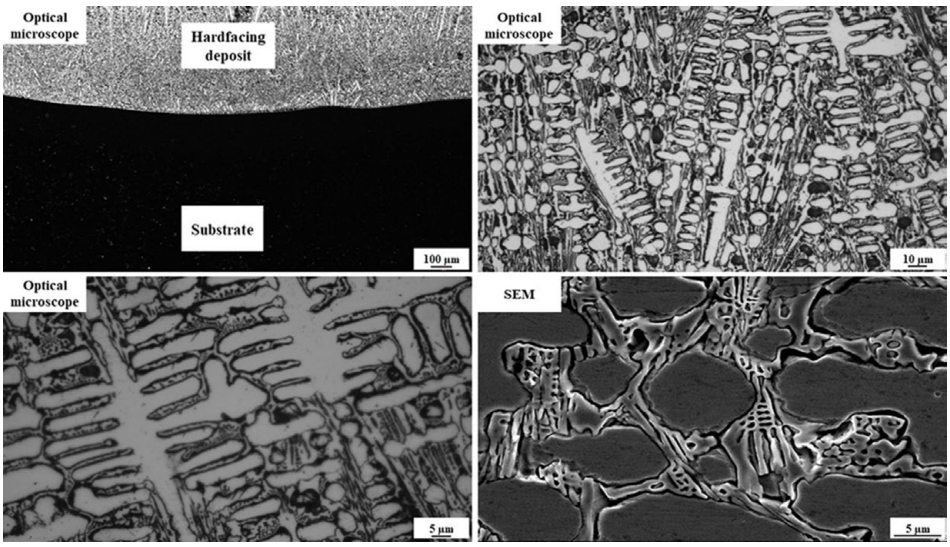

Fig. 7. Optical microscope and SEM microstructure images of hardfacing deposit sample # 3

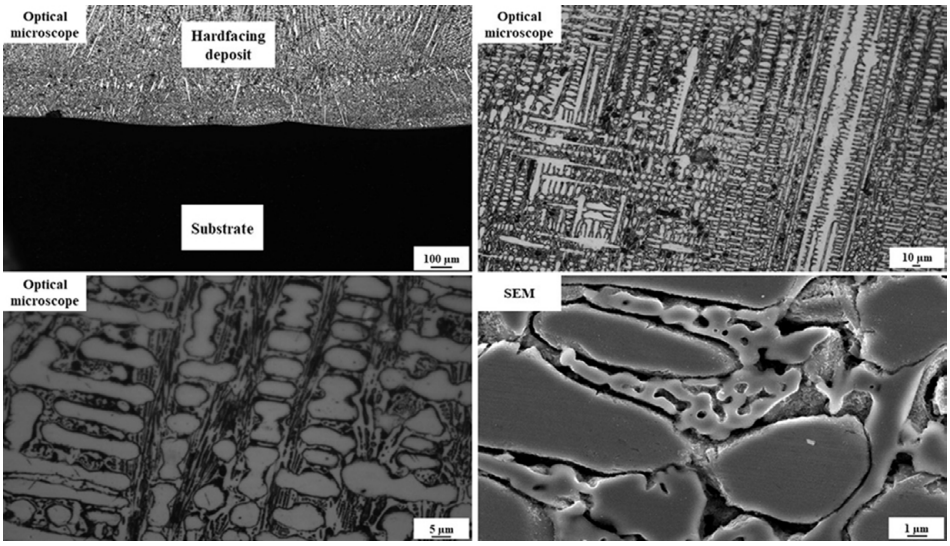

Fig. 8. Optical microscope and SEM microstructure images of hardfacing deposit sample # 4

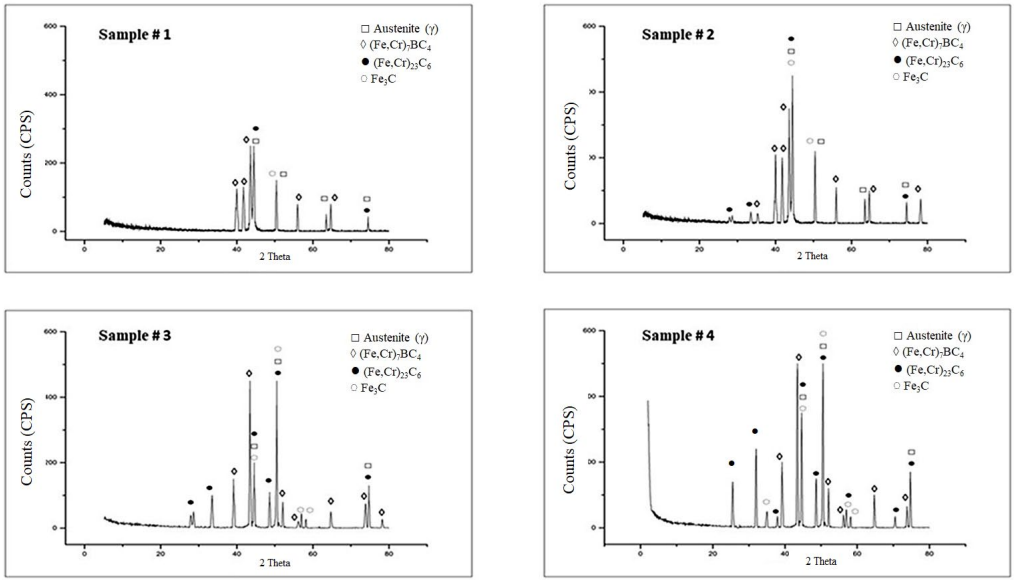

Fig. 9. XRD analysis results of hardfacing deposits

In microstructures, it was seen that carbides and boro-carbides containing iron and chromium were formed and these structures were sequenced near the austenite particles. The amount of these carbides and boro-carbides increased by the increase in the amount of ferrochromium and ferroboron in welding fluxes were determined. While the lowest density of carbides and boro-carbides was observed in the hardfacing deposit obtained by welding flux containing 4 wt.% ferrochromium and 2 wt.% ferroboron, the highest density of carbides and boro-carbides was observed in the hardfacing deposit obtained by welding flux containing 16 wt.% ferrochromium and 2 wt.% ferroboron.

In the microstructures of the hardfacing deposits, different phases formed depending on the percentages of iron, chromium, carbon, and boron in chemical composition analyses. During the solidification of hardfacing deposits, very hard, primary carbides (boro-carbides), $(Fe,Cr)_7BC_4$ formed in the welding pool as a first due to the presence of boron and relatively lower rates of chromium, iron, and carbon. After the primary carbides, the metallic matrix, austenite (γ iron) phases solidified from the remaining melt, while secondary carbides, $(Fe,Cr)_{23}C_6$ formed in the areas rich in iron and chromium and relatively lower rates of carbon via solid-state transformations. Similarly, eutectic carbides formed with eutectic reactions. The remaining chromium, boron, and carbon from these carbides and boro-carbides dissolved in the austenite phase as a retained austenite and formed the latest microstructures. All the austenite matrix was sequenced around and near the carbides and boro-carbides and took their places in the microstructures with different dendritic structures [9,27,29,30].

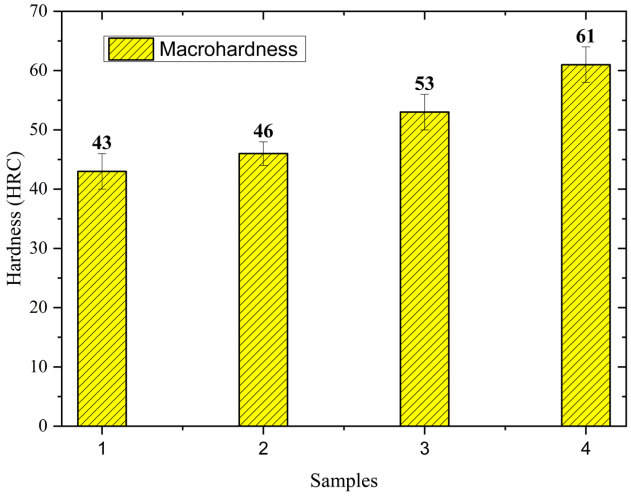

Fig. 10. Rockwell hardness results of hardfacing deposits

3.3. Hardness test results

The Rockwell hardness measurement results taken from 10 different areas of the hardfacing deposits and calculated as mean values are given in Fig. 10 and the Vickers hardness results measured by taking from 10 different transverse and longitudinal areas are given in Fig. 11. In Rockwell hardness measurements, while the highest hardness value (61 HRC) was observed in a hardfacing deposit obtained with welding flux containing 16 wt.% ferrochromium and 2 wt.% ferroboron, the lowest hardness value (43 HRC) was observed in a hardfacing deposit obtained with welding flux containing 4 wt.% ferrochromium and 2 wt.% ferroboron. As can be seen from the results of the Rockwell and Vickers hardness examinations, the hardness of the hardfacing deposits also increased by the increasing of chromium, carbon, and boron content in hardfacing deposits and accordingly, increasing of carbides and boro-carbides distribution in hardfacing deposit microstructures. As the percentages of chromium, carbon, and boron transitions from welding fluxes to the hardfacing deposits increased, the rates of carbide and boro-carbide phases in microstructures also increased. Thus, the hardness linearly increased due to the increasing rates of hard phase distribution in hardfacing deposit microstructures.

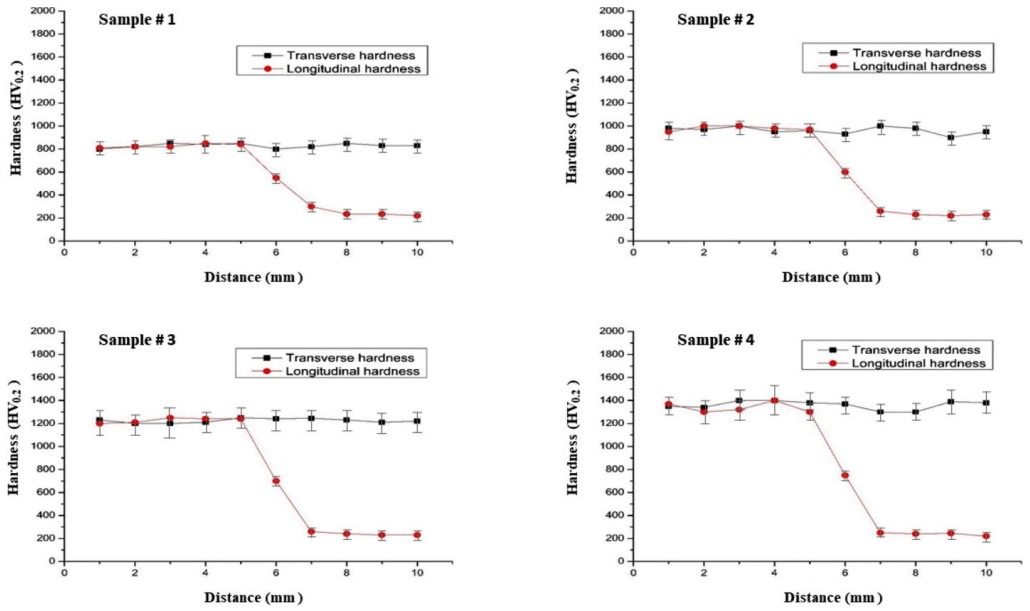

Fig. 11. Transverse and longitudinal Vickers hardness results of hardfacing deposits

In Fig. 12, while the carbide and boro-carbide phases present in the hardfacing deposits had a hardness-increasing effect, the austenite phase had a hardness-decreasing effect were determined [6,9,27-29]. Researchers in the literature conducted hardfacing deposits containing chromium, carbon, and boron via welding techniques and obtained similar hardness results to this study [6,9,27-29]. However, in the literature, no study using ferroalloys such as ferrochromium and ferroboron in submerged arc welding flux was found.

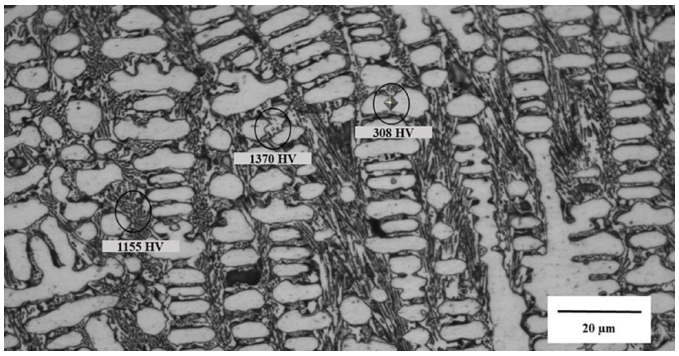

Fig. 12. Phase Vickers hardness measurements performed on hardfacing deposit sample # 2

As a result of the microhardness measurements taken from the hardfacing deposits, a homogeneous hardness distribution was obtained almost in all hardfacing deposit samples. This situation was associated with the austenite phase which was stable at room temperature and the presence of austenite phases that were tightly spread near the carbide and boro-carbide particles. The presence of very hard carbides and boro-carbides particles arranged in a very tight and grifted manner to austenite phases led to similar hardness results and thus, homogeneous results. Similarly, the presence of the austenite phase as a single phase in the microstructures of hardfacing deposits at room temperature contributed significantly to homogeneity. The absence of a phase such as a martensite [31] formed depending on the cooling rate in the hardfacing deposit microstructures contributed to obtain more homogeneous results. Similarly, the effects of high heat input on hardfacing deposits were minimal due to the absence of a phase such as martensite. In addition, the fact that all the phases in the microstructures were intensely located near the austenite particles contributed to obtaining more homogeneous results. The hardness difference between the phases in the hardfacing deposits caused partially non-homogeneous microhardness results by forming local differences in the microhardness results. This situation is seen in the hardfacing deposit sample # 4.

3.4. Abrasive wear test results

Fig. 13 shows the wear rate results of hardfacing deposits and Fig. 14 shows the SEM images obtained from the worn surfaces. When the wear rate results were examined, it was determined that the highest wear rate of 5.79 (10^{-7} mm^3 (N m)$^{-1}$) was observed in a hardfacing deposit obtained with welding flux containing 4 wt.% ferrochromium and 2 wt.% ferroboron, the lowest wear rate of 4.43 (10^{-7} mm^3 (N m)$^{-1}$) was observed in hardfacing deposit obtained with welding flux containing 16 wt.% ferrochromium and 2 wt.% ferroboron. Carbides and boro-carbides have hardness increasing effect, while austenite has a hardness-decreasing effect. Thus, with the increasing rates of carbides and boro-carbides in the microstructures, hardness values increased, and accordingly this situation caused a decrease in the wear losses by increasing the wear resistance in parallel with the effect of the elastic modulus and friction coefficient [4,6,9,26-28]. However, this comparison was carried out by ignoring the elastic modulus and friction coefficient.

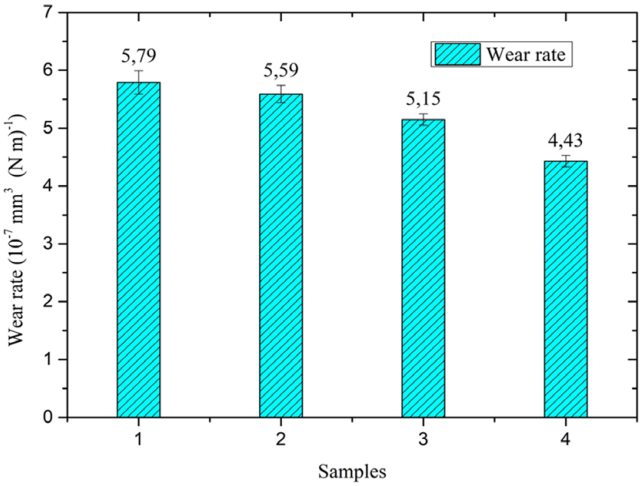

Fig. 13. Wear rate results of hardfacing deposits

When the worn surfaces in Fig. 14 were assessed in terms of the wear type, it was seen that wear types occurred as micro-cutting and micro-ploughing. The existence of such types of mechanisms was confirmed with the formation of continuous-discontinuous scratches and the crater gaps (cavities) due to the resistance of metallic matrix, hard carbides, and boro-carbides to the cutting and ploughing. When the SEM photographs of the worn surfaces were examined in terms of the surface characteristics, the presence of dense continuous scratches on the worn surface was observed in Fig. 14-sample # 1. In Fig. 14-sample # 2; the continuous scratches partially decreased and the presence of discontinuous scratches and numerous craters on the worn surface was observed. In Fig. 14-sample # 3; also dense discontinuous scratches and craters on the worn surface were observed. In Fig. 14-sample # 4; the scratches became very thin and that there were numerous crater dents were observed. Differences in wear scratches and the formation of craters are related to the number of carbides and boro-carbides in hardfacing deposits. Hardfacing deposits containing low percentages of chromium, carbon, and boron in chemical compositions have lower hardness and relatively lower wear resistance due to low carbide and boro-carbide ratios in microstructures. Thus, wear scratches formed in these types of hardfacing deposits mainly consist of continuous scratches, partially discontinuous scratches,

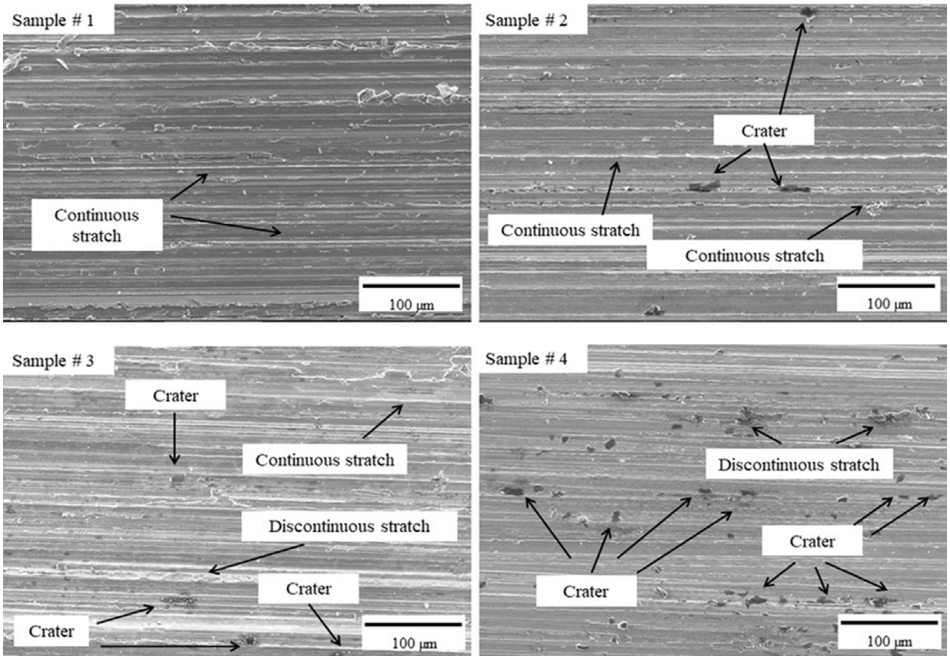

Fig. 14. Worn surface SEM images of hardfacing deposits

and craters. Hardfacing deposits containing high percentage of chromium, carbon, and boron in chemical compositions have higher hardness values and higher abrasion resistances due to the high carbide and boro-carbide ratios in microstructures [26-28]. For this reason, wear scratches formed in these types of hardfacing deposits mainly consist of thinner continuous scratches, discontinuous scratches, and more crater cavities.

4. Conclusions

Within the scope of the study, submerged arc welding fluxes containing increasing amounts of ferroalloys were produced for hardfacing deposit purposes. By using such welding fluxes prepared, hardfacing deposition processes were carried out on AISI 1020 steel surfaces. After the hardfacing deposition processes, slag properties of welding fluxes and surface properties of the hardfacing deposits were investigated. Besides, chemical composition, microstructure, hardness, and wear tests were performed to the characterization of the hardfacing deposits were carried out. According to these results;

1. All the welding fluxes had +300-500 µm particle size on average, and there were no faults such as porosities and cracks affecting the welding quality on the hardfacing deposit surfaces were determined.
2. With the increasing of ferroalloy percentages in the welding fluxes, the tendencies of the slags layer formed after welding processes to adhere to the weld metals increased and the separation times of the slags from the weld metals increased were observed.
3. The amounts of 1.54-6.84 wt.% chromium, 0.87-1.08 wt.% carbon, and 0.38-0.44 wt.% boron transition from welding fluxes to the hardfacing deposits were observed.
4. The structures targeted in the produced hardfacing deposits such as carbides and boro-carbides were observed.
5. With the increasing ratios of phases such as carbides and boro-carbides formed in hardfacing deposit microstructures, hardness results increased from 43 HRC to 61 HRC.
6. Due to the high wear resistance and high hardness value (61 HRC) of hardfacing deposit sample # 4, this hardfacing deposit can be used in wear applications requiring very high hardness values were recommended.

Acknowledgment

This work was supported by a grant from the scientific and technological research council of Turkey, TUBITAK (Project No: 114M016). The authors acknowledge the laboratory staff of the department of metallurgical and materials engineering from Firat University, TR for performing an effort to set up experimental design.

REFERENCES

[1] M. Nagentrau, A.L. Mohd Tobi, M. Sambu, S. Jamian, The Influence of Welding Condition on the Microstructure of WC Hardfacing Coating on Carbon Steel Substrate. Int. J. Refract. Met. H. **82**, 43-57 (2019).
DOI: https://doi.org/10.1016/j.ijrmhm.2019.03.029

[2] G.S. Ham, D.Y. Wi, S.H. Park, K.A. Lee, Effect of High-Frequency Heat Treatment on the Microstructure and Macroscopic Properties of WC-50Ni+Stellite 1 Coating Layer Fabricated by HVOF Spray Process. Arch. Metall. Mater. **65**, 1087-1092 (2020).
DOI: https://doi.org/10.24425/amm.2020.133222

[3] K.W. Kim, Y.K. Kim, S.H. Park, K.A. Lee, Laser Cladding of WC/T-800 Cermet: Fabrication, Microstructure, and Wear Properties. Arch. Metall. Mater. **66**, 713-717 (2021). DOI: https://doi.org/10.24425/amm.2021.136367

[4] H.Z. Oo, P. Muangjunburee, Wear Behaviour of Hardfacing on 3.5% Chromium Cast Steel by Submerged Arc Welding. Mater. Today: Proc. **5**, 9281-928 (2018). DOI: https://doi.org/10.1016/j.matpr.2017.10.101

[5] M. Kılıç, Microstructural Characterization of Ni-Based B_4C Reinforced Composite Coating Produced by tungsten Inert Gas Method. Arch. Metall. Mater. **66**, 917-924 (2021). DOI: https://doi.org/10.24425/amm.2021.136398

[6] M.H. Amushahi, F. Ashrafizadeh, M. Shamanian, Characterization of Boride-rich Hardfacing on Carbon Steel by Arc Spray and GMAW Processes. Surf. Coat. Technol. **204**, 2723-2728 (2010). DOI: https://doi.org/10.1016/j.surfcoat.2010.02.028

[7] E.N. Eremin, A.S. Losev, Wear Resistance Increase of Pipeline Valves by Overlaying Welding Flux-cored Wire. Procedia Eng. **113**, 435-440 (2015). DOI: https://doi.org/10.1016/j.proeng.2015.07.324

[8] M. Zhang, M. Li, J. Chi, S. Wang, L. Ren, M. Fang, Microstructure and Tribology Properties of In-situ MC(M:Ti,Nb) Coatings Prepared via PTA Technology. Vacuum **160**, 264-271 (2019). DOI: https://doi.org/10.1016/j.vacuum.2018.11.035

[9] R. Zahiri, R. Sundaramoorthy, P. Lysz, C. Subramanian, Hardfacing Using Ferro-alloy Powder Mixtures by Submerged Arc Welding. Surf. Coat. Technol. **260**, 220-229 (2014). DOI: https://doi.org/10.1016/j.surfcoat.2014.08.076

[10] B. Srikarun, H.Z. Oo, S. Petchsang, P. Muangjunburee, The Effects of Dilution and Choice of Added Powder on Hardfacing Deposited by Submerged Arc Welding. Wear **424-425**, 246-254 (2019). DOI: https://doi.org/10.1016/j.wear.2019.02.027

[11] K. Yang, Z. Zhang, W. Hu, Y. Bao, Y. Jiang, A New Type of Submerged-arc Flux-cored Wire Used for Hardfacing Continuous Casting Rolls. J. Iron Steel Res. Int. **18**, 74-79 (2011). DOI: https://doi.org/10.1016/S1006-706X(11)60120-9

[12] B. Srikarun, P. Muangjunburee, The Effect of Iron-based Hardfacing with Chromium Powder Addition onto Low Carbon Steel. Mater. Today: Proc. **5**, 9272-9280 (2018). DOI: https://doi.org/10.1016/J.MATPR.2017.10.100

[13] V.V. Golovko, N. Potapov, Special Features of Agglomerated (Ceramic) Fluxes in Welding. Weld. Int. **25**, 11, 889-893 (2011). DOI: https://doi.org/10.1080/09507116.2011.581431

[14] R. Oates, M.A. Saitta, Welding Handbook, Materials and Applications, Miami, FL, 33126, American Welding Society, 2000.

[15] https://www.magmaweld.com.tr/sw-701/uo/7985

[16] K.A. Reddy, Non-destructive Testing, Evaluation of Stainless Steel Materials. Mater. Today: Proc. **4**, 7302-7312 (2017). DOI: https://doi.org/10.1016/j.matpr.2017.07.060

[17] ASTM G132-96, Standard Test Method for Pin Abrasion Testing, ASTM International, West Conshohocken, PA, 2018.

[18] R. Mugele, H.D. Evans, Droplet Size Distribution in Sprays, J. Indst. and Eng. Chem. **43**, 1317-1324 (1951). DOI: https://doi.org/10.1021/ie50498a023

[19] https://www.lincolnelectric.com/en-us/consumables/submerged-arc/Pages/submerged-arc.aspx

[20] https://www.esabna.com/us/en/products/filler-metals/submerged-arc-wires-fluxes-saw/cladding-fluxes/index.cfm

[21] https://www.magmaweld.com/subarc-wires-fluxes/o/40

[22] B. Singh, Z.A Khan, A.N. Siddiquee, Review on Effect of Flux Composition on Its Behavior and Bead Geometry in Submerged Arc Welding (SAW). Int. J. Eng. Res. Technol. **7**, 12-12 (2013).

[23] T. Coetsee, F.J. De Bruin, Reactions at The Molten Flux-Weld Pool Interface in Submerged Arc Welding. High Temp. Mater. Process. **40**, 421-427 (2021). DOI: https://doi.org/10.1515/htmp-2021-0051

[24] A.V. Yarovchuk, Effect of Ferrochrome Content on The Oxidation-Reduction Processes in Welding Slags Based on Titanium Dioxide. Weld. Int. **19** (8), 651-656 (2005). DOI: https://doi.org/10.1533/wint.2005.3502

[25] N.A. Kozyrev, R.E. Kryukov, V.Y. Bendre, N.E. Kryukov, I.N. Kovalskiy, Carbon-containing Additions For Welding Fluxes. Weld. Int. **31** (5), 369-373 (2017). DOI: https://doi.org/10.1080/09507116.2016.1263459

[26] H. Lin, L. Ying, L. Jun, L. Binghong, Microstructure and Mechanical Properties for TIG Welding Joint of High Boron Fe-Ti-B Alloy. Rare Metal Mat. Eng. **43**, 283-286 (2014). DOI: https://doi.org/10.1016/S1875-5372(14)60059-X

[27] N. Yüksel, S. Sahin, Wear Behavior–Hardness–Microstructure Relation of Fe–Cr–C and Fe–Cr–C–B Based Hardfacing Alloys. Mater. Des. **58**, 491-498 (2014). DOI: https://doi.org/10.1016/J.MATDES.2014.02.032

[28] M. Kirchgaßner, E. Badisch, F. Franek, Behaviour of Iron-Based Hardfacing Alloys under Abrasion and Impact. Wear **265**, 772-779 (2008). DOI: https://doi.org/10.1016/j.wear.2008.01.004

[29] H.Berns, A. Fischer, Microstructure of Fe-Cr -C-B Alloys Addition of Nb, Ti and B. Metallography **20**, 401-429 (1987).

[30] J. Lippold C, D.J. Kotecki, Welding Metallurgy and Weldability of Stainless Steel, Wiley Interscience, John Wiley and Sons Inc. Publication, ISBN O-471-47379-0, 10-12 (2005).

[31] C. Du, J.P.M. Hoefnagels, S. Kölling, M.G.D. Geers, J. Sietsma, R. Petrov, V. Bliznuk, P.M. Koenraad, D. Schryvers, B. Amin-Ahmadi, Martensite Crystallography and Chemistry in Dual Phase and Fully Martensitic Steels. Mater. Charact. **139**, 411-420 (2018). DOI: https://doi.org/10.1016/j.matchar.2018.03.011